

RESEARCH ARTICLE

D PepH3, an Improved Peptide Shuttle for Receptor-independent Transport Across the Blood-Brain Barrier

Marco Cavaco^{1,2}, Javier Valle², Ruben da Silva³, João D. G. Correia³, Miguel A. R. B Castanho¹, David Andreu^{2,*} and Vera Neves^{1,*}

¹Instituto de Medicina Molecular, Faculdade de Medicina, Universidade de Lisboa, Av Prof Egas Moniz, 1649-028 Lisboa, Portugal;

²Proteomics and Protein Chemistry Unit, Department of Experimental and Health Sciences, Pompeu Fabra University, Barcelona, Spain; ³Centro de Ciências e Tecnologias Nucleares and Departamento de Engenharia e Ciências Nucleares, Instituto Superior Técnico, Universidade de Lisboa, CTN, Estrada Nacional 10 (km 139,7), 2695-066 Bobadela LRS, Portugal

Abstract: *Background:* The use of peptides as drug carriers across the blood-brain barrier (BBB) has increased significantly during the last decades. PepH3, a seven residue sequence (AGILKRW) derived from the α -helical domain of the dengue virus type-2 capsid protein, translocates across the BBB with very low toxicity. Somehow predictably from its size and sequence, PepH3 is degraded in serum relatively fast. Among strategies to increase peptide half-life ($t_{1/2}$), the use of the enantiomer (wholly made of *D*-amino acid residues) can be quite successful if the peptide interacts with a target in non-stereospecific fashion.

Methods: The goal of this work was the development of a more proteolytic-resistant peptide, while keeping the translocation properties. The serum stability, cytotoxicity, *in vitro* BBB translocation, and internalization mechanism of D PepH3 was assessed and compared to the native peptide.

Results: D PepH3 demonstrates a much longer $t_{1/2}$ compared to PepH3. We also confirm that BBB translocation is receptor-independent, which fully validates the enantiomer strategy chosen. In fact, we demonstrate that internalization occurs through macropinocytosis. In addition, the enantiomer demonstrates to be non-cytotoxic towards endothelial cells as PepH3.

Conclusion: D PepH3 shows excellent translocation and internalization properties, safety, and improved stability. Taken together, our results place D PepH3 at the forefront of the second generation of BBB shuttles.

ARTICLE HISTORY

Received: October 28, 2019
Accepted: January 23, 2020

DOI:

10.2174/1381612826666200213094556

Keywords: Adsorption-mediated transcytosis, blood-brain barrier, *D*-amino acids, macropinocytosis, PepH3, peptide shuttles, stability.

1. INTRODUCTION

The integrity of the blood-brain barrier (BBB) is crucial for homeostasis of the central nervous system (CNS) [1]. Disruption of BBB integrity is critical in the progression of diseases such as Alzheimer's (AD), Parkinson's (PD), or multiple sclerosis (MS), among others [2]. Treatment of these conditions requires the delivery of therapeutic drugs by BBB translocation, a challenging task as only 2% of described drugs can cross the BBB [3].

Among the various approaches to traverse the BBB [4], the safest include: 1) transporters, such as those for glucose or amino acids; 2) receptors, such as those for transferrin or insulin; and 3) modulation of BBB biophysical properties, such as charge or lipid composition [5]. Approaches 1 and 2 above, namely carrier-mediated transcytosis (CMT) and receptor-mediated transcytosis (RMT), respectively, have important limitations such as saturation and interference with the biochemical processes associated to the natural ligands [4, 6], potentially disturbing brain homeostasis. In addition, the same carriers/receptors may be present in other body regions, thus leading to off-target interactions with adverse effects [7, 8]. In contrast, approach 3, also known as adsorptive-mediated transcytosis (AMT), does not have the intrinsic limitations of transporters and receptors. AMT is typically effected by positively

charged peptide shuttles that mediate translocation by electrostatic interaction with negatively charged proteoglycans [9, 10], forming vesicles that transport the conjugates across the endothelial cell network layer [11].

Recently, our group has shown that viral proteins are an interesting source of cell-penetrating peptides (CPPs) [12]. Dengue virus type-2 is particularly relevant as some short sequences of its capsid protein (DEN2C) translocate endothelial cells by receptor-independent routes [13, 14]. We performed a systematic study of the α -helical domains of DENC2 and were able to identify a peptide, named PepH3, with very good brain penetration both *in vitro* and *in vivo* [15]. The ability of PepH3 to carry large cargos across the BBB was tested using a cellular *in vitro* BBB model, which showed $31.91 \pm 3.02\%$ translocation of PepH3-conjugated GFP after 5 h [16]. PepH3 was also conjugated to anti- β -amyloid protein 42 (bAP42) single-domain antibody (sdAb) (anti-bAP42 sdAb) and evaluated *in vivo* [17]. Biodistribution studies in healthy mice revealed significant brain uptake of radiolabeled PepH3 at 5 min post-injection: $0.31 \pm 0.07\%$ injected dose per gram of tissue (ID/g of tissue). Interestingly, the conjugate showed a brain accumulation of $1.5 \pm 0.50\%$ ID/g at PepH3. In addition, only $0.04 \pm 0.01\%$ ID/g of the conjugate was found in the brain at 1h post-injection, suggesting that peptide is capable of returning to the bloodstream. However, none of these studies addressed the stability of the molecules.

The high proteolytic degradation rate represents a major drawback in peptide drug development [18] and several strategies have been explored to overcome this issue in the last decade [19, 20]. Among them, the use of *D*-amino acids has been one of the most frequently applied. *D*-peptides display higher resistance towards

*Address correspondence to these authors at the Instituto de Medicina Molecular, Faculdade de Medicina, Universidade de Lisboa, Av. Prof Egas Moniz, 1649-028 Lisboa, Portugal; Tel: +217985136; E-mail: veraneves@medicina.ulisboa.pt
Proteomics and Protein Chemistry Unit, Department of Experimental and Health Sciences, Pompeu Fabra University, Barcelona, Spain; Tel: 34-933160868; Fax: 34-933160901; E-mail: david.andreu@upf.edu

Table 1. Peptides synthesized.

Peptide	Amino Acid Sequence ¹	Modification	Mass (Da), Calculated (Found)	HPLC t _R (min) ²	Purity (%)
PepH3	AGILKRW-amide	None	842.8 (843.0)	5.5	99.5
CF-PepH3	CF-AGILKRW-amide	Fluorophore	1202.2 (1201.4)	6.3	96.3
_D PepH3	aGilk _r w-amide	<i>D</i> -enantiomer	842.8 (842.5)	5.7	99.8
CF- _D PepH3	CF-aGilk _r w-amide	<i>D</i> -enantiomer + fluorophore	1202.2 (1201.2)	6.1	95.8

¹By convention, *D*-residues are shown in lower case; *L*-residues and (non-chiral) Gly in upper case.

²See experimental part for details.

enzymatic degradation than their natural counterparts, thus having increased half-life times ($t_{1/2}$). In the present work, the stability of _DPepH3 in human serum was compared to that of PepH3 and the translocation efficacy mechanism was studied as well.

2. MATERIALS AND METHODS

2.1. Peptide Synthesis and Purification

PepH3 (AGILKRW-amide) and _DPepH3 (aGilk_rw-amide) were made in a Prelude synthesizer (Gyros Protein Technologies, Tucson, AZ) running Fmoc (FastMoc) SPPS protocols at 0.1 mmol scale on a Fmoc-Rink-amide ChemMatrix resin (Table 1). Sidechain functionalities were protected with N^G-2,2,4,6,7-pentamethylidihydrobenzofuran-5-sulfonyl (Arg), and N^α-tert-butylloxycarbonyl (Lys, Trp) groups. Eight-fold excess of Fmoc-*L*- or Fmoc-*D*-amino acids and HBTU, in the presence of a double molar amount of DIEA, were used for the coupling steps, with DMF as a solvent. After chain assembly, full deprotection and cleavage were carried out with TFA/H₂O/TIS (95:2.5:2.5, v/v, 90 min, room temperature (r.t.)). The fluorescent analogues of both peptides were similarly synthesized (Table 1). Briefly, 5(6)-carboxyfluorescein (CF) was coupled manually to the protected peptide-resin with 4-fold excess in the presence of an equivalent amount of DIPCDI in DMF. After deprotection and cleavage with TFA/H₂O/TIS (95:2.5:2.5, v/v, 90 min, r.t.), peptides were isolated by precipitation with cold diethyl ether and centrifugation at 4,000 ×g, 4 °C for 20 min, taken up in H₂O and lyophilized.

Analytical reversed-phase HPLC was performed on a Luna C18 column (4.6 mm × 50 mm, 3 μm; Phenomenex, USA). Linear gradients of solvent B (0.036% TFA in MeCN) into solvent A (0.045% TFA in H₂O) were used at a flow rate of 1 mL/min and with UV detection at 220 nm. Preparative HPLC runs were performed on a Luna C18 column (21.2 mm × 250 mm, 10 μm; Phenomenex) using linear gradients of solvent B (0.1% TFA in MeCN) into solvent A (0.1% TFA in H₂O) at a flow rate of 25 mL/min and with UV detection at 220 nm. Fractions of adequate HPLC homogeneity and with the expected mass were combined and lyophilized. LC-MS was performed in a LC-MS 2010EV instrument (Shimadzu, Kyoto, Japan) fitted with an XBridge C18 column (4.6 mm × 150 mm, 3.5 μm; Waters, Spain), eluting with linear gradients of HCOOH/MeCN (0.08% v/v) into HCOOH/H₂O (0.1% v/v) over 15 min at 1 mL/min. Peptide stock solutions (1 mM) in filtered H₂O were stored at -20°C.

2.2. Large Unilamellar Vesicles (LUVs)

LUVs were prepared as described before [21, 22]. Briefly, the lipid mixture was dissolved in chloroform in a round bottom flask, chloroform was evaporated under a constant nitrogen flow and the resulting lipid film was dried in vacuum overnight (o.n.). A multilamellar vesicle suspension (MLV) was obtained after lipid film rehydration with 10 mM sodium phosphate (75.4 mM Na₂HPO₄, 24.6 mM NaH₂PO₄, pH 7.4) and 10 freeze/thaw cycles. MLV suspensions were extruded through a 100 nm track-etched polycar-

bonate membrane (Whatman, United Kingdom) in a LiposoFast-Basic plus Stabilizer setup (Avestin, Germany). POPC, POPC:POPS (3:2), and POPC:POPS (1:4) mixtures were prepared. LUV hydrodynamic diameter (D_H) and sample polydispersity were characterized by dynamic light scattering (DLS).

2.3. Circular Dichroism

Circular dichroism (CD) spectra of the different peptides were acquired in a J-815 spectropolarimeter (Jasco, Japan) at 25°C in the 190-260 nm wavelength range, with a bandwidth of 1 nm and a scan speed of 50 nm/min, using a 0.1 cm quartz cell [23]. 50 μM peptide solutions were prepared in 10 mM sodium phosphate (75.4 mM Na₂HPO₄, 24.6 mM NaH₂PO₄, pH 7.4) in the absence or presence of 2 mM lipid vesicles (POPC, POPC:POPS (3:2), or POPC:POPS (1:4)) (Sigma-Aldrich, Spain). The final spectra for each peptide were the average of three consecutive scans per sample after the subtraction of buffer baselines. Results were expressed as mean residue ellipticity ($[\theta]_{MRW}$) (deg × cm² × dmol⁻¹), as follows:

$$[\theta]_{MRW} = \frac{(\theta_{obs} \times MRW)}{10dc} \quad \text{Equation 1}$$

where θ_{obs} is the observed ellipticity in degrees, MRW is the mean residue weight, d is the cell path length and c is the peptide molar concentration.

2.4. Hemolytic Assays

Fresh human blood was collected in EDTA tubes and centrifuged at 1000 ×g for 10 min at 4°C. The supernatant was discharged and the pellet containing red blood cells (RBCs) was washed three times with 1× PBS (137 mM NaCl, 2.7 mM KCl, 10 mM Na₂HPO₄, and 1.8 mM KH₂PO₄, pH 7.4) and suspended in 1× PBS to obtain a 1.0% (v/v) suspension. Then, RBCs were added to centrifuge tubes containing 2-fold serially diluted peptides to a final concentration ranging from 0.01 to 100 μM. The suspension was incubated for 24 h at 37°C with gentle stirring. After that, the samples were centrifuged for 2 min at 1000 ×g. Supernatants were transferred to 96-well plates, and the hemoglobin released measured by absorbance at 570 nm in an Infinite F200 TECAN plate reader [24]. 1× PBS with no peptides and Triton X-100 at 1% and 4% (v/v) were used as negative and positive controls, respectively. Hemolytic activity (%) was determined using the following equation:

$$\text{Hemolytic activity (\%)} = \frac{\text{Abs}_{PT} - \text{Abs}_{NC}}{\text{Abs}_{PC} - \text{Abs}_{NC}} \quad \text{Equation 2}$$

where Abs_{PT} is the absorbance of treated samples, Abs_{NC} is the absorbance from negative control, and Abs_{PC} absorbance from positive control.

HC₅₀ values were determined using the GraphPad Prism 7.0 software using a log(inhibitor) vs. normalized response. Experiments were performed on different days using independent blood donors.

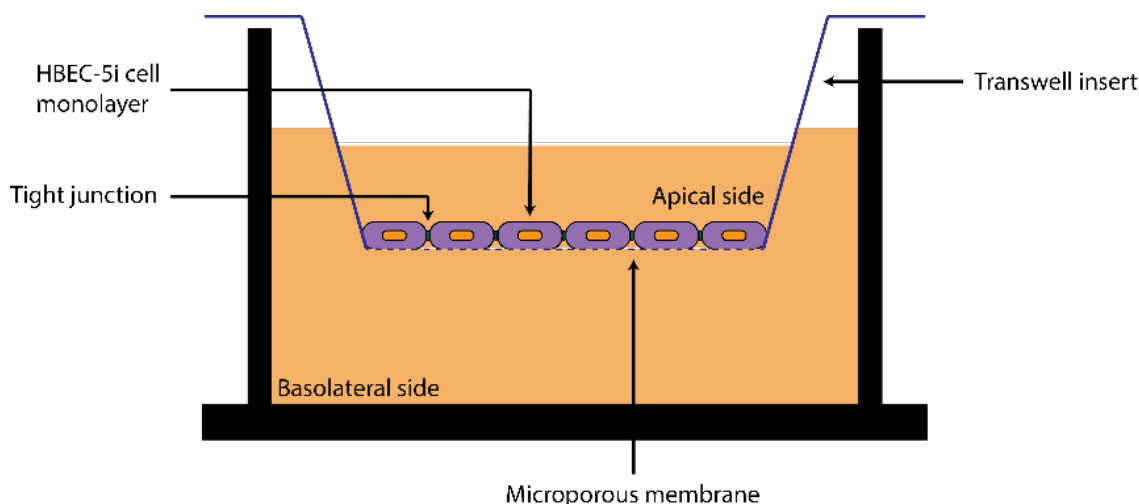


Fig. (1). *In vitro* BBB model representation. The *in vitro* BBB model consists of a transwell system with an insert in which HBEC-5i cells are grown in two separate chambers. The insert, or apical side, corresponds to the blood side, while the basolateral side (bottom chamber) corresponds to the brain side. (A higher resolution / colour version of this figure is available in the electronic copy of the article).

2.5. Serum Stability

Aliquots (500 μ L) of human serum (Sigma-Aldrich, Spain) and peptide (1 mM in H₂O) were incubated for 2 h at 37°C with gentle swirling. At different time points (0, 1, 5, 10, 30, 60, and 120 min), 120 μ L aliquots were taken and treated with 120 μ L of 96% ethanol for 30 min at 4°C, and centrifuged at 13,000 rpm for 10 min to remove serum proteins [25]. The supernatant was analyzed by HPLC on a PerkinElmer Series 200 on a Luna C18 column (4.6 mm \times 50 mm, 3 μ m, Phenomenex, USA), eluting with linear gradients of HCOOH/MeCN (0.1%, v/v) into HCOOH/H₂O (0.1%, v/v) over 15 min at 1 mL/min. UV detection was at 220 nm.

2.6. Cell Culture

Human cerebral microvascular endothelial cells (HBEC-5i, ATCC[®] CRL-3245) were cultured as a monolayer on 0.1% gelatin (Gibco/ Thermo Fisher, USA)-coated T-flasks in DMEM:F12. The medium was supplemented with 10% fetal bovine serum (FBS), 1% penicillin/streptomycin (Gibco/Thermo Fisher, USA), and 40 μ g/mL endothelial growth supplement (ECGS) (Sigma-Aldrich, Spain), according to the manufacturer’s instructions. Cells were grown in a humidified atmosphere of 5% CO₂ at 37°C (MCO-18AIC (UV), Sanyo, Japan), with the medium changed every other day.

2.7. Cell Proliferation Assay

The cytotoxicity of PepH3 and _DPepH3 towards HBEC-5i cells was determined using CellTiter-Blue[®] Cell Viability Assay (Promega, USA), according to the manufacturer’s instructions. The assay is based on the ability of viable cells to reduce resazurin into resorufin, a highly fluorescent metabolite. Non-viable cells are not able to generate resorufin. Using this approach, it is possible to distinguish between metabolic and non-metabolic cells, and indirectly determine the cytotoxicity of different compounds. HBEC-5i cells were seeded onto gelatin pre-coated well plates (Corning, USA) at 20,000 cells/100 μ L/well and incubated for 24 h. After medium removal, 100 μ L of previously diluted peptides (0.01 - 100 μ M) in DMEM:F12 medium were added to the wells. After 24 h incubation with peptides, 20 μ L CellTiter-Blue[®] reagent was added to each well and incubated for 3 h in a humidified atmosphere of 5% CO₂ at 37°C. The fluorescence intensity was measured with excitation and emission λ of 560 and 590 nm, respectively, using an Infinite F200 TECAN plate reader. Medium and 1% Triton X-100-containing medium were used as a positive control (100% cell via-

bility) and negative control (0% cell viability), respectively. HBEC-5i cell viability (%) was determined using the following equation:

$$\text{Cell Viability (\%)} = \frac{F_p - F_{NC}}{F_{PC} - F_{NC}} \times 100 \quad \text{Equation 3}$$

where F_p is the fluorescence intensity of peptide-treated cells, F_{NC} that for negative controls, and F_{PC} that for positive controls. Experiments were performed on different days using independently grown cell cultures.

2.8. In vitro BBB Translocation Assay

An *in vitro* BBB model consisting of endothelial cells growing on the apical side of a porous membrane was used [26, 27]. HBEC-5i cells were allowed to grow until confluence in a culture T-flask. Then, cells were carefully harvested with trypsin-EDTA (Gibco/ Thermo Fisher, USA) and seeded (8,000 cells/well) onto gelatin-coated tissue culture 24-well inserts (transparent polyester membrane with 1.0 μ m pores) (BD Falcon, USA). The medium was changed every other day for 8 days, after which cells were washed twice with 1 \times PBS and once with DMEM:F12 medium without phenol red (Gibco/Thermo Fisher, USA). Then, peptides diluted in DMEM:F12 without phenol red to a final concentration of 1 μ M were added to the apical side of the *in vitro* BBB model (Fig. 1). Experiments were performed on different days using independently grown cell cultures.

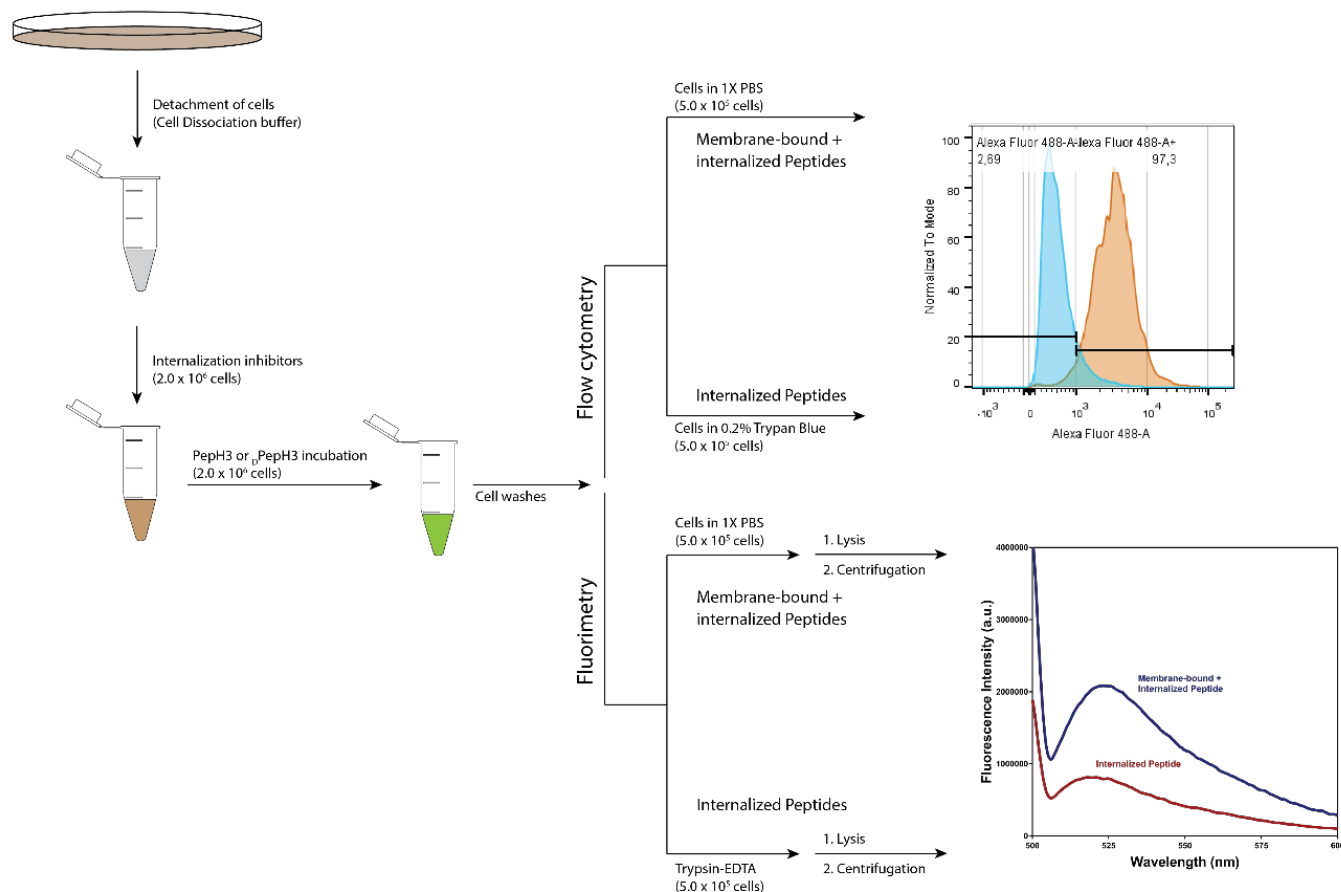
The translocation of 5(6)-carboxyfluorescein-labeled peptides (CF-PepH3 and CF-_DPepH3) was determined by fluorescence emission. After 24 h incubation, samples from the apical and basolateral side were collected and analyzed. Fluorescence was measured using an Infinite F200 TECAN plate reader. The percentage (%) of translocation was calculated using the following equation:

$$\text{Translocation (\%)} = \left(\frac{F_i - F_{\text{cells}}}{F_{\text{peptide}}} \right) \times 100 \quad \text{Equation 4}$$

where F_i is the recovered fluorescence intensity, F_{cells} is the recovered fluorescence intensity from cells without peptide, and F_{peptide} is the fluorescence intensity of total peptide initially added to the transwell apical side.

2.9. In vitro BBB Integrity Assay

After 24 h incubation with peptides, an *in vitro* integrity assay was performed [15]. Briefly, cells were washed twice with 1 \times PBS and once with DMEM:F12 medium without phenol red. Then, previously diluted fluorescein isothiocyanate-dextran with an MW of 4 kDa (FD4) (Sigma-Aldrich, Spain) was added to the apical side and incubated for 2 h. FD4 was diluted in DMEM:F12 medium without



Scheme 1. Protocol used to quantify the relative and absolute amount of peptides internalized in HBEC-5i cells after incubation with different endocytic and non-endocytic inhibitors. Adapted from [28]. (A higher resolution / colour version of this figure is available in the electronic copy of the article).

phenol red to an absorbance of 0.1. Samples were collected from the apical and basolateral side, and fluorescence intensity was measured with excitation and emission λ of 560 and 590 nm, respectively, using an Infinite F200 TECAN plate reader. The integrity of the barrier was determined as follows:

$$\text{Integrity (\%)} = 100 - \left(\frac{F_i - F_{\text{cells}}}{F_{\text{FD4}} - F_{\text{Medium}}} \times 100 \right) \quad \text{Equation 5}$$

where F_i is the recovered fluorescence intensity, F_{cells} is the recovered fluorescence intensity from cells without FD4 incubation, F_{FD4} is the fluorescence intensity of total FD4 initially added to the transwell apical side, and F_{Medium} is the fluorescence intensity of DMEM:F12 medium without phenol red.

2.10. Evaluation of the Internalization Mechanism

A protocol described elsewhere was used to quantify peptide internalization by flow cytometry and fluorimetry (Scheme 1) [28]. Briefly, HBEC-5i cells were harvested after the confluence with cell dissociation buffer (Gibco/Thermo Fischer, USA), centrifuged at $1,000 \times g$ for 10 min and suspended in DMEM:F12 medium. To assess the internalization pathway, cells (2.0×10^6) were treated with different internalization inhibitors for 1 h (Table 2), then incubated with 100 μL of peptide (10 μM in DMEM:F12 medium). After incubation, cells were centrifuged at $1,000 \times g$, 4°C , for 10 min, the cell pellet was washed with cold $1 \times$ PBS, centrifuged at $1,000 \times g$ and resuspended in 800 μL . One half of the suspension was used to quantify peptide internalization by flow cytometry (see below), the other half to quantify internalization by fluorimetry (Scheme 1).

To analyze internalization by flow cytometry, one half of the cell suspension (500,000 cells/(200 μL)) was used to measure the

total fluorescence (membrane-bound + internalized peptide). The other half was treated with 0.2% Trypan Blue (Gibco/Thermo Fischer, USA) to quench membrane-bound fluorescence (internalized peptide). The fluorescence intensity of 20,000 cells was analyzed with a BD LSRFortessa X-20 flow cytometer. The mean fluorescence of a sample was obtained by subtracting the autofluorescence of cells from the measured mean fluorescence of cells in the presence of fluorescent peptide.

For quantification by fluorimetry, half of the cell suspension (500,000 cells/200 μL) was incubated with trypsin-EDTA for 5 min at 37°C to hydrolyze membrane-bound (internalized) peptide. After addition of 100 μL of enzyme inhibitors (Roche, USA) diluted in 0.1% BSA to a final concentration expressed on Table 2 for 1h, cells were transferred to a centrifuge tube, centrifuged ($2,000 \times g$, 10 min), washed with 1 mL of 50 mM Tris, pH 7.4, 0.1% BSA, and lysed in 200 μL 50 mM Tris, pH 7.4, 1M NaCl, 1% NP40. The samples were then sonicated for 30 min and centrifuged for 10 min at $16,000 \times g$. To obtain the total amount of cell-associated peptide (membrane-bound + internalized peptide), cells were directly lysed in 200 μL 50 mM Tris pH 7.4, 1M NaCl, 1% NP40, sonicated for 30 min and centrifuged for 10 min at $16,000 \times g$. Fluorescence intensity in the supernatants was monitored with an FS900 fluorometer (Edinburgh Instruments, UK) between 500 and 600 nm (0.2 sec/0.5 nm). The maximal intensity detected (ca. 520 nm) was used to build a calibration curve for subsequent sample quantification. The amounts of total or internalized peptide were calculated by referring to the fluorescence intensity of the sample to the calibration curve. Samples for the calibration curve were prepared in parallel. All experiments were performed in duplicates and repeated at least three independently.

Table 2. Inhibitors of internalization used in different assays. Inhibitors and mechanism of inhibition used in the experiments are listed below.

Inhibitor ^a	Reference	Action	Concentration
Incubation at 4°C	-	ATP-dependent endocytosis	-
Dynasore hydrate	Sigma-Aldrich, Spain	Dynamin dependent vesicle formation	50 μM
Chlorpromazine hydrochloride (CPZ)	Sigma-Aldrich, Spain	Clathrin pits	50 μM
Methyl-β-cyclodextrin (MβCD)	Sigma-Aldrich, Spain	Lipid rafts / caveolae	5 mM
Amiloride (EIPA)	Sigma-Aldrich, Spain	Macropinocytosis	50 μM
Phloretin	Sigma-Aldrich, Spain	Reduction of membrane dipole potential	30 μM
Heparinase	Sigma-Aldrich, Spain	Digestion of heparin sulfate proteoglycan	0.6 UN
Brefeldin A	Sigma-Aldrich, Spain	Golgi vesicle formation	10 μg/mL

^aAll the inhibitors were incubated for 1h prior to peptide addition.

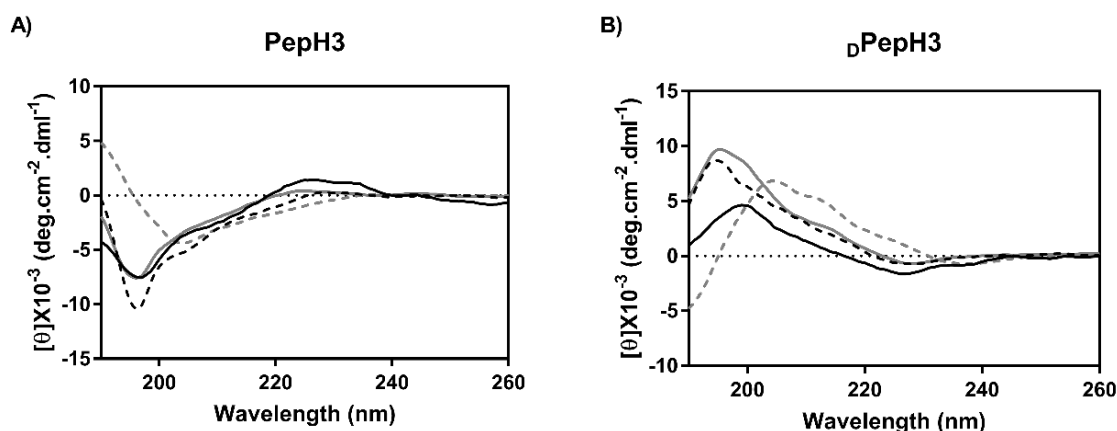


Fig. (2). Secondary structure of peptides. CD spectra of (A) PepH3 and (B) D -PepH3 in aqueous buffer (black solid line), in contact with POPC vesicles (black dashed line), POPC:POPS (3:2) vesicles (grey solid line), and POPC:POPS (1:4) vesicles (grey dashed line). (A higher resolution / colour version of this figure is available in the electronic copy of the article).

2.11. Confocal Microscopy

HBEC-5i cells were seeded (25,000 cells/200 μL) on an ibi-Treat-coated 8-well μ-slide (Ibidi, Germany) for 24 h, then washed carefully twice with 1× PBS and once with medium and incubated for 1 h with labeled peptides at a final concentration of 10 μM. After 1 h, cells were washed again twice with 1× PBS and once with medium and nucleus was stained with Hoechst 33342 (Thermo Fisher, USA) at a final concentration of 5 μg/mL for 10 min at 37°C. Finally, cells were washed twice with 1× PBS and imaged.

The acquisition was made on a confocal point-scanning Zeiss LSM 880 microscope (Carl Zeiss, Germany) equipped with an alpha Plan-Apochromat X 20 dry objective (0.80 numerical aperture). Diode 405-30 was used to excite Hoechst 33342 (Sigma-Aldrich, Spain). The 488 nm line from an Ar laser was used to excite peptide labeled with CF. In the normal confocal mode, × 0.6 zoom images were recorded at 3440 × 3440 resolution. ZEN and Fiji softwares were used for image acquisition and image processing, respectively. At least 12 total images were acquired in three independent replicates.

2.12. Statistical Analysis

All data points are presented as mean ± standard deviation (SD) of results obtained on different days and repeated at least two times. Statistical significance was calculated by applying one-way ANNO-

VA followed by Dunnett's multiple comparison test, and nonparametric Mann-Whitney, Kruskal-Wallis and two-tailed unpaired *t*-tests. *** *p*-value < 0.001, ** *p*-value < 0.01, * *p*-value < 0.05. GraphPad Prism 7.0 software package was used for quantitative data processing.

3. RESULTS

3.1. Secondary Structure of Peptides

The conformational features of PepH3 and D -PepH3 were studied by CD (Fig. 2). The spectrum of PepH3 reveals a single negative band with a minimum at 195 nm in aqueous buffer or in either POPC or POPC:POPS (3:2) vesicles, which shifts to 205 nm in POPC:POPS (1:4) vesicles (Fig 2A). The spectrum of D -PepH3 is the mirror image of PepH3, as expected from its composition in *D*-amino acids (Fig. 2B). While the spectral signatures of both peptides in aqueous or POPC or POPC:POPS (3:2) media are characteristic of random-coil conformation, in POPC:POPS (1:4) vesicles, which mimic the lipid composition of endothelial cells [29], the observed shift to 205 nm minimum/maximum is characteristic of α -helical structure. This vesicle type-induced conformational shift plausibly bears upon the translocation capabilities of both peptides.

3.2. Serum Stability

The susceptibility to proteolysis in human serum was evaluated for both peptides. Fig. (3A) shows proteolysis kinetics for PepH3

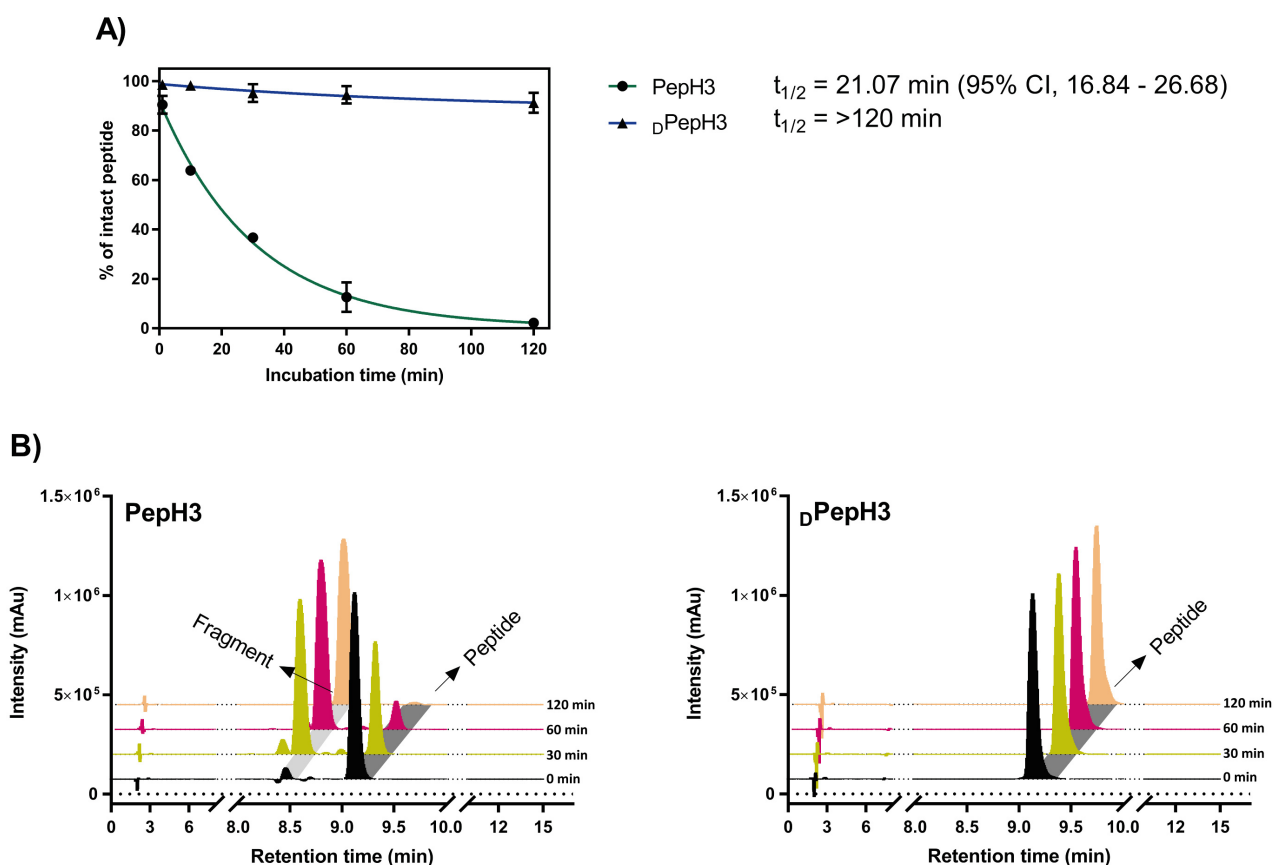


Fig. (3). Stability of PepH3 and $_D$ PepH3 in 50% (v/v) human serum. (A) Peptide extinction curves obtained from chromatogram peak integration for PepH3 and $_D$ PepH3 in human serum. The $t_{1/2}$ s were calculated by fitting the experimental data to an exponential decay model. Data points in the plot are the mean of three experiments and the corresponding 95% CI is shown. (B) Elution profiles after peptide incubation with 50% (v/v) human serum at representative times (0, 30, 60, and 120 min), using a 0% - 95% ACN gradient over 15 min. (A higher resolution / colour version of this figure is available in the electronic copy of the article).

and $_D$ PepH3 obtained by the integration of chromatograms in Fig. (3B), as well as the $t_{1/2}$ obtained from regression fitting. For a small peptide rich in basic residues, PepH3 was rather stable to proteolysis, with $t_{1/2} = 21.07$ min. LC-MS analysis showed the most substantial cleavage to occur at the Lys-Arg bond, giving rise to the fragments AGILK-carboxyl and RW-amide. As expected, $_D$ PepH3 was basically impervious to degradation, with ~90% unaltered at the longest incubation time tested (120 min).

3.3. Cytotoxic Activity

Toxicity of PepH3 and $_D$ PepH3 towards healthy cells was evaluated in two ways: (i) in a hemolysis assay, both peptides failed to induce hemolysis of human erythrocytes up to 100 μ M (Fig. 4A). In contrast, melittin, a well-known membranolytic peptide used as a positive control, showed a low HC_{50} of 6.17 ± 1.48 μ M; (ii) toxicity was also assessed towards the HBEC-5i brain endothelial cells used in the *in vitro* BBB model, in order to understand the possible effect of both peptides on BBB integrity. Again, neither peptide was shown to be toxic up to 100 μ M after 24 h incubation (Fig. 4B).

3.4. *In vitro* BBB Translocation and Integrity Evaluation

The translocation capabilities of both peptides were evaluated by adding 5(6)-carboxyfluorescein-labeled peptides (CF-PepH3 and CF- $_D$ PepH3) to the apical (top) chamber of the *in vitro* BBB model (Fig. 1). The apical and basolateral (bottom) side volumes were recorded after 24 h, and the fluorescence of each chamber measured.

As expected, PepH3 was shown to efficaciously translocate the BBB model, with up to $52.98 \pm 4.36\%$ of fluorescence found in the

bottom chamber after 24 h (Fig. 5A). A $34.02 \pm 4.39\%$ retained peptide, resulting from internalization and membrane binding, was concurrently found. $_D$ PepH3 followed a similar pattern, with $49.35 \pm 3.50\%$ and $40.38 \pm 3.32\%$ BBB translocation and retention, respectively (Fig. 5A). The comparable *in vitro* translocation profiles suggest a receptor-free mechanism for both peptides. Moreover, the rather similar peptide contents (40-50%) found at each chamber of the transwell device (Fig. 1) for both PepH3 and $_D$ PepH3 strongly suggest an equilibrium distribution, in tune with an AMT mechanism.

The integrity of the endothelial barrier was evaluated by the leakage of fluorescently labeled 4 kDa dextran (FD4) (Fig. 5B) [30]. Outflow of fluorescent probe from the apical side in the presence or absence of peptide was negligible, which demonstrated the lack of peptide-induced fenestration or paracellular leakage.

3.5. Mechanism of Peptide Cellular Internalization

A systematic analysis of potential peptide internalization mechanisms of PepH3 and $_D$ PepH3 across HBEC-5i cells was undertaken by selective inhibition of one or more traffic pathways. The internalization of both peptides was significantly challenged by low temperature (4°C) (Fig. 6A1, B1), clearly hinting at energy-dependent uptake. Next, endocytosis inhibitors (Dynasore [31], CPZ [31], M β CD [32], and EIPA [33]) were tested, of which only EIPA caused a significant drop in internalization for both PepH3 and $_D$ PepH3, suggesting that macropinocytosis is playing an active role in translocation. Internalization was also hampered by phloretin [34] and brefeldin A [35] (Fig. 6). The first inhibitor reduces

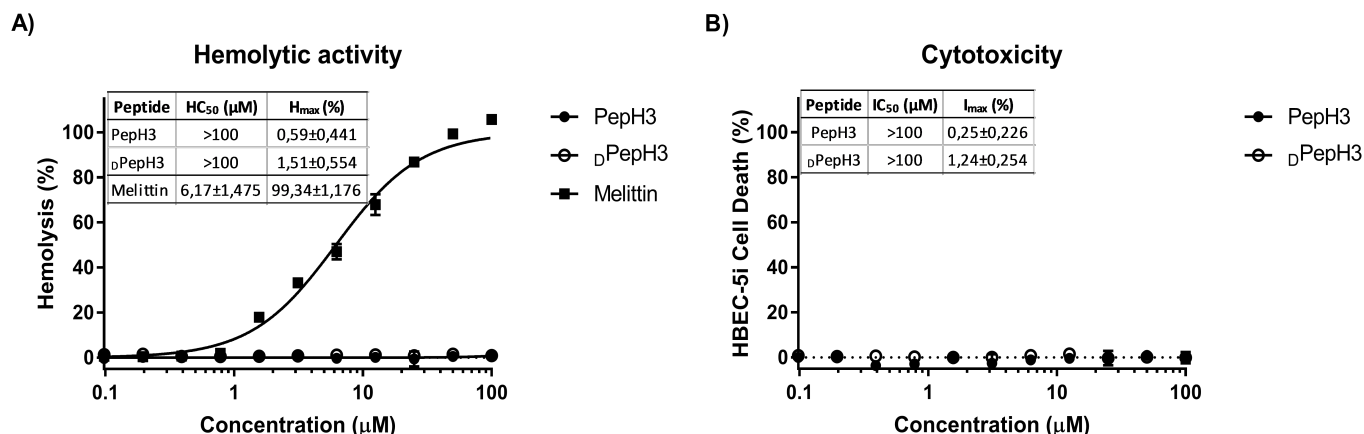


Fig. (4). *In vitro* toxicity. (A) To evaluate the toxicity of PepH3 and DPEpH3 against RBCs as healthy cell models, an RBC suspension (1.0%, v/v) was incubated with 0.01 to 100 µM peptide for 24 h. Hemolysis (%) was determined by the absorbance of hemoglobin released into the supernatant. Melittin was included as a positive control (B) The cytotoxicity of both peptides against HBEC-5i cells was also assessed with the same 0.01 to 100 µM concentration range for 24 h. Cell death (%) was determined using a CellTiter® Blue reagent assay. The experiment was repeated on different days using independently grown cell cultures. No statistical significant differences were found in either hemolytic activity or cytotoxicity between PepH3 and DPEpH3.

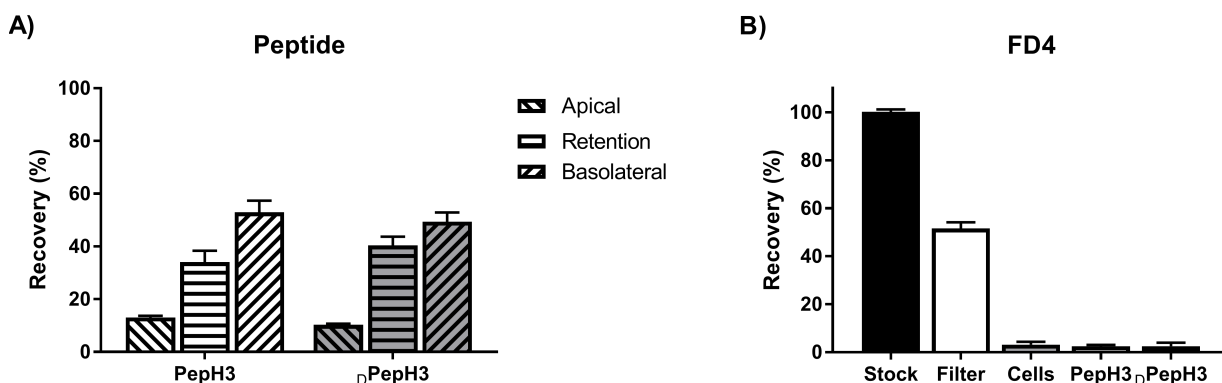


Fig. (5). *In vitro* BBB translocation. (A) Translocation in an *in vitro* transwell BBB model. A total of 1 µM of 5(6)-carboxyfluorescein-labeled peptides (CF-PepH3 and CF-DPEpH3) was initially added to the apical (top) side. After 24h incubation, the amount of PepH3 (white bars) and DPEpH3 (grey bars) in the apical and basolateral (bottom) side were quantified, referred to the initial amount added (at top) and expressed as percentage of recovered fluorescence at either compartment. Retention is defined as the difference (in %) between the initial (100%) and the aggregated top and bottom amounts. (B) Determination of transwell *in vitro* BBB integrity. After 24 h incubation, FD4 (MW 4 kDa) fluorescence intensity in the basolateral compartment was measured in the absence (“Cells” bar) or the presence of peptides, and referred to the amount of FD4 initially added to the top. Controls (leftmost bars) were the FD4 stock solution and the naked filter (no cells attached). Data are from triplicates of three independent experiments. No statistical significant differences were found in either translocation of the peptide (basolateral) or FD4 between PepH3 and DPEpH3. (A higher resolution / colour version of this figure is available in the electronic copy of the article).

membrane dipole potential, affecting membrane charge. The later affects Golgi trafficking, which intervenes in vesicle formation and, consequently, on peptide internalization and exocytosis. The results obtained with fluorimetry were in line with those from flow cytometry (Fig. 6A2, B2), both at low temperature and with endocytic inhibitors.

3.6. Peptide Intracellular Localization

To investigate how peptides were distributed within cells, confocal microscopy was performed on HBEC-5i cells after incubation with CF-PepH3 and CF-DPEpH3 for 1 h. Images in Fig. (7) show both peptides inside the cells, demonstrating internalization. The comparable fluorescence intensities observed for PepH3 and DPEpH3 suggest that the peptides have similar structures and efficacies upon translocation.

4. DISCUSSION

The use of CPPs as delivery systems to increase the concentration of therapeutic agents in the CNS is an active field of research

[36]. Our group has contributed to it with the discovery of PepH3, a seven residue peptide derived from DEN2C [15] and shown to efficiently penetrate the brain, either in free form or conjugated to proteins [15-17]. As with many other peptides [37, 38], PepH3 is rather susceptible to proteolysis, with $t_{1/2}$ = 21.07 min (Fig. 3). To address this limitation, the D-amino acid version of the peptide, DPEpH3, was made and shown to be practically impervious to proteolysis, $t_{1/2}$ > 120 min (Fig. 3), as proteases do not recognize peptides with D-residues [39, 40] (Fig. 8A).

Although mechanisms driving CPP internalization and BBB translocation do not always receive adequate attention [41, 42], this information is valuable to understand the selectivity and toxicity of these peptides. Herein, we used a systematic approach to explore the pathways of PepH3 and DPEpH3 across the BBB. Some CPP sequences have been found to be quite efficient in BBB translocation by receptor-independent routes [13, 14], where no enantioselective discrimination applies [43, 44]. This is indeed also the case for DPEpH3, for which uptake levels quite comparable to the

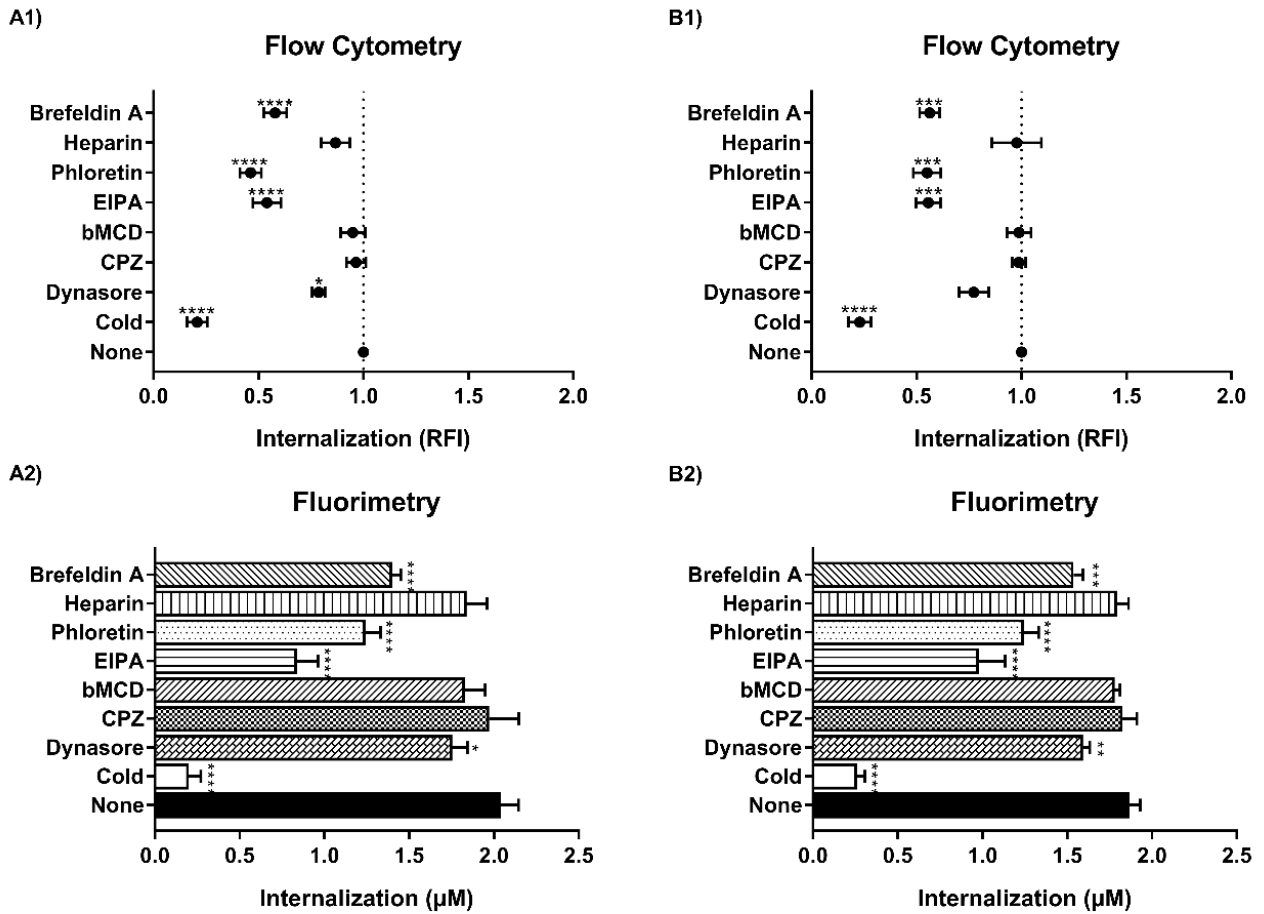


Fig. (6). Internalization Mechanism. HBEC-5i cells were incubated with different inhibitors for 1 h at 37°C, as detailed in Table 1. Then, PepH3 (A1 - A2) and D^{N} PepH3 (B1 - B2) at 10 μM were added to cells and incubated for 1 h at 37°C or 4°C (“Cold”). After incubation, cells were distributed into centrifuge tubes and analyzed by flow cytometry (A1 and B1) or fluorimetry (A2 and B2). A one-way ANOVA statistical test followed by a Dunnett’s test was used to compare each condition with cells without inhibitor (“None”). (* $p \leq 0.05$; ** $p \leq 0.01$; *** $p \leq 0.001$; **** $p \leq 0.0001$). All experiments were performed in duplicates and repeated at least twice independently.

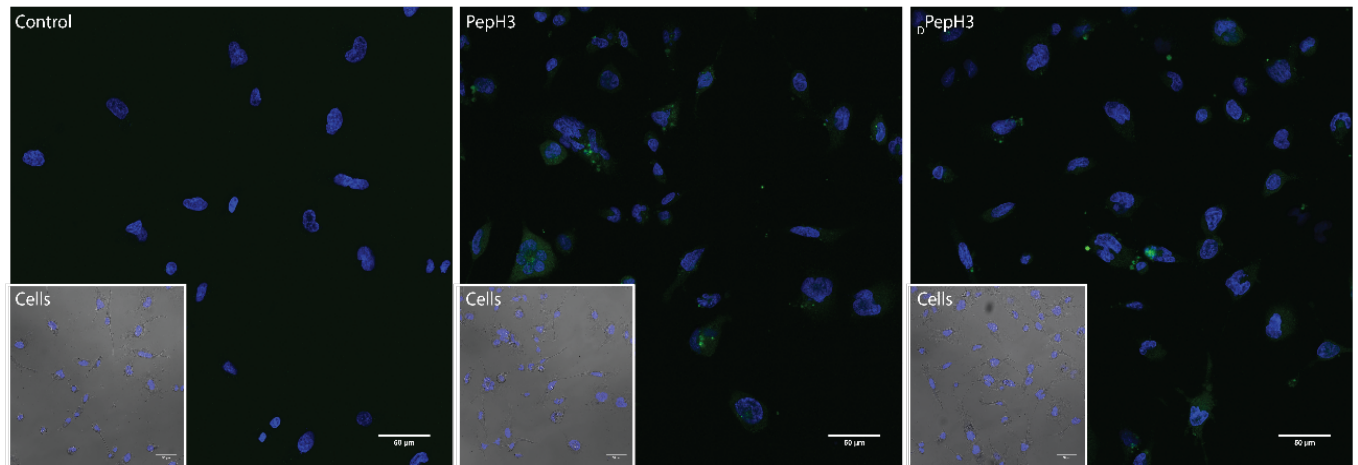


Fig. (7). Confocal microscopy of PepH3 and D^{N} PepH3. HBEC-5i cells were treated with 10 μM of peptides for 1h at 37°C. Cell morphology can be visualized with bright field (left corner). Nuclei are stained with Hoechst (blue) and CF- labeled peptides appear in green. Bar represents 50 μm. (A higher resolution / colour version of this figure is available in the electronic copy of the article).

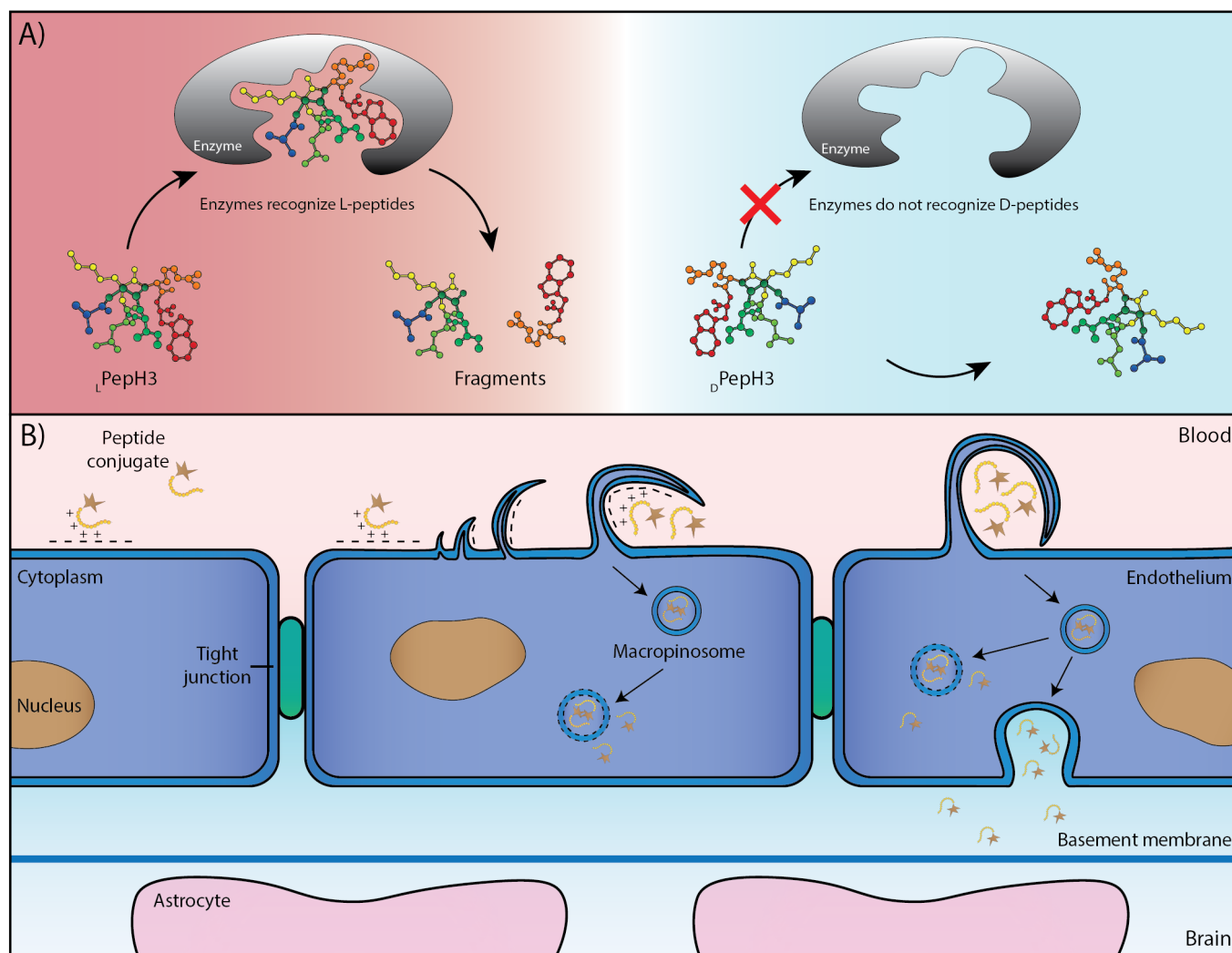


Fig. (8). Representation of the different mechanisms behind peptide internalization, and protease resistance. **(A)** Scheme of the protease resistance mechanism responsible for the long half-life of the enantiomer. Enzymes are stereoselective, thus, they recognize specific peptide conformations. By changing peptide from L to D amino acids, enzymes are not able to recognize peptides with the same affinity. **(B)** Schematic representation of the transcytosis of extracellular peptide conjugated to a protein cargo in endothelial cells. Firstly, by electrostatic interaction between positive charge peptide and negative charge endothelial cells, peptide interacts with an endothelial membrane. Secondly, the conjugate is uptake *via* macropinosytosis. Finally, inside the cell, the conjugate might be either released into the cytoplasm or continue intracellular traveling and be released on the opposite side of the endothelial cell (transcytosis). (A higher resolution / colour version of this figure is available in the electronic copy of the article).

enantiomer ($49.35 \pm 3.50\%$ vs. $52.98 \pm 4.36\%$, respectively) have been determined (Fig. 5), the statistically non-significant difference in percentage thus ruling out RMT. Also, the roughly equal amounts (ca. 50%) of either PepH3 or *D*PepH3 at each of the transwell chambers strongly suggest an equilibrium distribution coherent with the reversible nature of an AMT mechanism. AMT is known to be triggered by electrostatic interaction between a cationic molecule and an anionic cell surface [9], as is the case with PepH3 and BECs [29]. The CD results showed that interaction with negatively charged lipids induces structuration as an α -helix for both PepH3 and *D*PepH3, which might increase their translocation propensity (Fig. 2). Further, in support of a non-receptor, electrostatically-driven AMT mechanism, PepH3 and *D*PepH3 adsorption onto BEC membranes were demonstrated using phloretin (Fig. 6), an inhibitor of the dipolar interaction at the membrane level [45-47].

Molecule uptake through membranes may occur through energy-independent or -dependent routes [48, 49]. The first route con-

sists of direct penetration, which is fast and impaired by low temperature (*e.g.*, 4°C) that reduces membrane fluidity [50, 51]. The second route includes pathways such as macropinosytosis, micropinosytosis, clathrin-dependent endocytosis and caveolae/lipid raft-mediated endocytosis, which can be elucidated by endocytosis-specific inhibitors (Table 1) [52, 53]. In our case, PepH3 internalization is inhibited at 4°C (Fig. 6), confirming an energy-dependent route. On the other hand, the macropinosytosis EIPA inhibitor significantly reduced internalization, suggesting that after initial PepH3 or *D*PepH3 electrostatic interaction with negatively charged BEC surfaces (Fig. 8B) a macropinosome is formed that traverses the BEC lumen and releases the peptide shuttle (and its cargo) at the other side of the endothelium.

Finally, both peptides are safe towards healthy human cells (Fig. 4) and do not interfere with BBB integrity (Fig. 5), an important feature for systemic administration and brain homeostasis.

“Giving the D-peptide properties: good translocation, good serum stability, and safety *in vitro*, we foresee its application *in*

vivo. First, to evaluate its pharmacokinetics parameters, such as AUC, Cl, and $t_{1/2}$, as well as organ biodistribution, with emphasis in its brain uptake. Secondly, to assess its application as delivery system to the brain, $_D$ PepH3 can be conjugate to a therapeutic molecule. The potential of the system will be confirmed by its efficacy in the treatment of a brain disease.”

CONCLUSION

In this work, we have addressed the limited serum half-life of PepH3 by exploring the structural and functional features of its *D*-version, a recognized strategy to enhance peptide stability. When conformationally defined (*i.e.*, in structure-promoting anionic lipid environment), the enantiomer $_D$ PepH3 was predictably the mirror image (a left-handed α -helix) of PepH3 and, not surprisingly, exceedingly more stable than the *L* version. The touchstone of this approach was obviously showing that the enantiomer strategy did not curtail the functional fitness of $_D$ PepH3 as a BBB shuttle. This was indeed the case, our results showing that both enantiomers display similar behaviors in their translocation and internalization mechanisms in a transwell *in vitro* BBB model. Differences in translocation levels were not statistically significant, consistent with receptor-independent uptake. Plus, the equilibrium distribution of peptide between both sides of the transwell setup, as well as the affinity towards anionic vesicles, support AMT as a translocation mechanism. Finally, when exploring the pathway of peptide internalization by two independent techniques, namely fluorimetry and flow cytometry, micropinocytosis emerged as a plausible route. Taken together, our results portray $_D$ PepH3 as an improved version of PepH3 that paves the way to a new generation of short, proteolysis resistant, efficacious peptide BBB shuttles.

LIST OF ABBREVIATIONS

Abs	=	Absorbance
AD	=	Alzheimer’s disease
AMT	=	Adsorptive-mediated transcytosis
bAP42	=	β -amyloid protein 42
BBB	=	Blood-brain Barrier
BEC	=	Brain endothelial cell
BSA	=	Bovine serum albumin
CD	=	Circular dichroism
CF	=	5(6)-carboxyfluorescein
CMT	=	Carrier-mediated transcytosis
CNS	=	Central nervous system
CPP	=	Cell-penetrating peptide
CPZ	=	Chlorpromazine hydrochloride
DEN2C	=	Dengue virus type-2 capsid protein
D_H	=	Hydrodynamic diameter
DIEA	=	<i>N,N</i> -Diisopropylethylamine
DIPCDI	=	<i>N,N'</i> -Diisopropylcarbodiimide
DLS	=	Dynamic light scattering
DMF	=	<i>N,N</i> -Dimethylformamide
ECGS	=	Endothelial growth supplement
EDTA	=	Ethylenediaminetetraacetic acid
EIPA	=	Amiloride
FBS	=	Fetal bovine serum
FD4	=	Fluorescein isothiocyanate-dextran with a MW of 4 kDa
HBEC-5i	=	Human cerebral microvascular endothelial cells
HBTU	=	<i>N,N,N',N'</i> -Tetramethyl-O-(1 <i>H</i> -benzotriazol-1-yl)uronium hexafluorophosphate

HPLC	=	High Performance Liquid Chromatography
LC-MS	=	Liquid chromatography–mass spectrometry
LUV	=	Large unilamellar vesicle
MLV	=	Multilamellar vesicle
MRW	=	Mean residue weight
MS	=	Multiple sclerosis
M β CD	=	Methyl- β -cyclodextrin
PBS	=	Phosphate buffer saline
POPC	=	1-palmitoyl-2-oleoyl-sn-glycero-3-phosphocholine
POPS	=	1-palmitoyl-2-oleoyl-sn-glycero-3-phospho-L-serine
r.t.	=	Room temperature
RBCs	=	Red blood cells
RMT	=	Receptor-mediated transcytosis
sdAb	=	Single-domain antibody
$t_{1/2}$	=	Half-life
TAT	=	Human Immunodeficiency Virus Trans-activator of transduction
TFA	=	Trifluoroacetic acid
TIS	=	Triisopropylsilane

ETHICS APPROVAL AND CONSENT TO PARTICIPATE

Not applicable.

HUMAN AND ANIMAL RIGHTS

No Animals/Humans were used for studies that are the basis of this research.

CONSENT FOR PUBLICATION

Not applicable.

AVAILABILITY OF DATA AND MATERIALS

The data that supports the findings of this study is available from the corresponding author, (Vera L. S. Neves) upon reasonable request.

FUNDING

The authors thank the Portuguese Fundação para a Ciência e a Tecnologia (FCT, grants PD/BD/128281/2017, PTDC/BBBNAN/1578/2014, UID/Multi/04349/2019 and PTDC/QUINUC/30147/2017), the Spanish Ministry of Economy and Innovation (MINECO, grants AGL2014-52395-C2-2-R, AGL2017-84097-C2-2-R and Maria de Maeztu Program for Centers of Excellence), Spain; the European Union H2020-MSCA-RISE-2014 program (grant no. 828774), and the “La Caixa” Banking Foundation (grant HR17-00409) for financial support.

CONFLICT OF INTEREST

The authors declare no conflict of interest, financial or otherwise.

ACKNOWLEDGEMENTS

Declared none.

REFERENCES

- [1] Serlin Y, Shelef I, Knyazer B, Friedman A. Anatomy and physiology of the blood-brain barrier. *Semin Cell Dev Biol* 2015; 38: 2-6. <http://dx.doi.org/10.1016/j.semcdb.2015.01.002> PMID: 25681530
- [2] Furtado D, Björnmalm M, Ayton S, Bush AI, Kempe K, Caruso F. Overcoming the blood-brain barrier: the role of nanomaterials in treating neurological diseases. *Adv Mater* 2018; 30(46): e1801362. <http://dx.doi.org/10.1002/adma.201801362> PMID: 30066406

- [3] Partridge WM. Blood-brain barrier delivery. *Drug Discov Today* 2007; 12(1-2): 54-61.
<http://dx.doi.org/10.1016/j.drudis.2006.10.013> PMID: 17198973
- [4] Gabathuler R. Approaches to transport therapeutic drugs across the blood-brain barrier to treat brain diseases. *Neurobiol Dis* 2010; 37(1): 48-57.
<http://dx.doi.org/10.1016/j.nbd.2009.07.028> PMID: 19664710
- [5] Neves V, Aires-da-Silva F, Corte-Real S, Castanho MARB. antibody approaches to treat brain diseases. *Trends Biotechnol* 2016; 34(1): 36-48.
<http://dx.doi.org/10.1016/j.tibtech.2015.10.005>
- [6] Partridge WM. Drug transport across the blood-brain barrier. *J Cereb Blood Flow Metab* 2012; 32(11): 1959-72.
<http://dx.doi.org/10.1038/jcbfm.2012.126> PMID: 22929442
- [7] Pulicherla KK, Verma MK. Targeting therapeutics across the blood brain barrier (BBB), prerequisite towards thrombolytic therapy for cerebrovascular disorders-an overview and advancements. *AAPS Pharm Sci Tech* 2015; 16(2): 223-33.
<http://dx.doi.org/10.1208/s12249-015-0287-z> PMID: 25613561
- [8] Pulgar VM. Transcytosis to cross the blood brain barrier, new advancements and challenges. *Front Neurosci* 2019; 12(1019): 1019.
<http://dx.doi.org/10.3389/fnins.2018.01019> PMID: 30686985
- [9] Hervé F, Ghinea N, Scherrmann J-M. CNS delivery via adsorptive transcytosis. *AAPS J* 2008; 10(3): 455-72.
<http://dx.doi.org/10.1208/s12248-008-9055-2> PMID: 18726697
- [10] Abdul Razzak R, Florence GJ, Gunn-Moore FJ. Approaches to CNS drug delivery with a focus on transporter-mediated transcytosis. *Int J Mol Sci* 2019; 20(12): 3108.
<http://dx.doi.org/10.3390/ijms20123108> PMID: 31242683
- [11] Kristensen M, Brodin B. Routes for drug translocation across the blood-brain barrier: exploiting peptides as delivery vectors. *J Pharm Sci* 2017; 3549(17): 30361-1.
- [12] Freire JM, Almeida Dias S, Flores L, Veiga AS, Castanho MARB. Mining viral proteins for antimicrobial and cell-penetrating drug delivery peptides. *Bioinformatics* 2015; 31(14): 2252-6.
<http://dx.doi.org/10.1093/bioinformatics/btv131> PMID: 25725499
- [13] Freire JM, Veiga AS, Conceição TM, *et al.* Intracellular nucleic acid delivery by the supercharged dengue virus capsid protein. *PLoS One* 2013; 8(12): e81450.
<http://dx.doi.org/10.1371/journal.pone.0081450> PMID: 24339931
- [14] Ma L, Jones CT, Groesch TD, Kuhn RJ, Post CB. Solution structure of dengue virus capsid protein reveals another fold. *Proc Natl Acad Sci USA* 2004; 101(10): 3414-9.
<http://dx.doi.org/10.1073/pnas.0305892101> PMID: 14993605
- [15] Neves V, Aires-da-Silva F, Morais M, *et al.* Novel peptides derived from dengue virus capsid protein translocate reversibly the blood-brain barrier through a receptor-free mechanism. *ACS Chem Biol* 2017; 12(5): 1257-68.
<http://dx.doi.org/10.1021/acscmbio.7b00087> PMID: 28263555
- [16] Neves-Coelho S, Eleutério RP, Enguita FJ, Neves V, Castanho MARB. A new noncanonical anionic peptide that translocates a cellular blood-brain barrier model. *Molecules* 2017; 22(10): 1753.
<http://dx.doi.org/10.3390/molecules22101753> PMID: 29057814
- [17] Côte-Real S, Neves V, Oliveira S, Canhão P, Outeiro T, Castanho M, Aires da Silva F. Antibody molecules and peptide delivery systems for use in Alzheimer's disease and related disorders. *World Intellectual Property Organization patent PCT/IB2016/050467*. 2016 Jan.
- [18] Wang B, Xie N, Li B. Influence of peptide characteristics on their stability, intestinal transport, and *in vitro* bioavailability: a review. *J Food Biochem* 2019; 43(1): e12571.
<http://dx.doi.org/10.1111/jfbc.12571> PMID: 31353489
- [19] Cavaco M, Castanho MARB, Neves V. Peptibodies: an elegant solution for a long-standing problem. *Biopolymers* 2017; 110(1): e23095.
<http://dx.doi.org/10.1002/bip.23095> PMID: 29266205
- [20] Vamanu E. Polyphenolic nutraceuticals to combat oxidative stress through microbiota modulation. *Front Pharmacol* 2019; 10(492): 492.
<http://dx.doi.org/10.3389/fphar.2019.00492> PMID: 31130865
- [21] Figueira TN, Freire JM, Cunha-Santos C, *et al.* Quantitative analysis of molecular partition towards lipid membranes using surface plasmon resonance. *Sci Rep* 2017; 7: 45647.
<http://dx.doi.org/10.1038/srep45647> PMID: 28358389
- [22] Figueira TN, Palermo LM, Veiga AS, *et al.* *In vivo* efficacy of measles virus fusion protein-derived peptides is modulated by the properties of self-assembly and membrane residence. *J Virol* 2016; 91(1): e01554-16.
PMID: 27733647
- [23] Falcao CB, Pérez-Peinado C, de la Torre BG, *et al.* Structural dissection of crotalicidin, a rattlesnake venom cathelicidin, retrieves a fragment with antimicrobial and antitumor activity. *J Med Chem* 2015; 58(21): 8553-63.
<http://dx.doi.org/10.1021/acs.jmedchem.5b01142> PMID: 26465972
- [24] Pérez-Peinado C, Dias SA, Domingues MM, *et al.* Mechanisms of bacterial membrane permeabilization by crotalicidin (Ctn) and its fragment Ctn(15-34), antimicrobial peptides from rattlesnake venom. *J Biol Chem* 2018; 293(5): 1536-49.
<http://dx.doi.org/10.1074/jbc.RA117.000125> PMID: 29255091
- [25] Ghosh A, Raju N, Tweedle M, Kumar K. *In vitro* mouse and human serum stability of a heterobivalent dual-target probe that has strong affinity to gastrin-releasing peptide and neuropeptide y1 receptors on tumor cells. *Cancer Biother Radiopharm* 2017; 32(1): 24-32.
<http://dx.doi.org/10.1089/cbr.2016.2136> PMID: 28186846
- [26] Helms HC, Abbott NJ, Burek M, *et al.* *In vitro* models of the blood-brain barrier: An overview of commonly used brain endothelial cell culture models and guidelines for their use. *J Cereb Blood Flow Metab* 2016; 36(5): 862-90.
<http://dx.doi.org/10.1177/0271678X16630991> PMID: 26868179
- [27] Czupalla CJ, Liebner S, Devraj K. *In vitro* models of the blood-brain barrier.cerebral angiogenesis: methods and protocols. New York, NY: Springer New York. 2014; 415-37.
http://dx.doi.org/10.1007/978-1-4939-0320-7_34
- [28] Illien F, Rodriguez N, Amoura M, *et al.* Quantitative fluorescence spectroscopy and flow cytometry analyses of cell-penetrating peptides internalization pathways: optimization, pitfalls, comparison with mass spectrometry quantification. *Sci Rep* 2016; 6: 36938.
<http://dx.doi.org/10.1038/srep36938> PMID: 27841303
- [29] Ribeiro MM, Domingues MM, Freire JM, Santos NC, Castanho MA. Translocating the blood-brain barrier using electrostatics. *Front Cell Neurosci* 2012; 6(44): 44.
PMID: 23087614
- [30] Gonzalez-Velasquez FJ, Kotarek JA, Moss MA. Soluble aggregates of the amyloid-beta protein selectively stimulate permeability in human brain microvascular endothelial monolayers. *J Neurochem* 2008; 107(2): 466-77.
<http://dx.doi.org/10.1111/j.1471-4159.2008.05618.x> PMID: 18702666
- [31] De Bock M, Van Haver V, Vandenbroucke RE, Decrock E, Wang N, Leybaert L. Into rather unexplored terrain-transcellular transport across the blood-brain barrier. *Glia* 2016; 64(7): 1097-123.
<http://dx.doi.org/10.1002/glia.22960> PMID: 26852907
- [32] Rodal SK, Skretting G, Garred O, Vilhardt F, van Deurs B, Sandvig K. Extraction of cholesterol with methyl-beta-cyclodextrin perturbs formation of clathrin-coated endocytic vesicles. *Mol Biol Cell* 1999; 10(4): 961-74.
<http://dx.doi.org/10.1091/mbc.10.4.961> PMID: 10198050
- [33] Fittipaldi A, Ferrari A, Zoppé M, *et al.* Cell membrane lipid rafts mediate caveolar endocytosis of HIV-1 Tat fusion proteins. *J Biol Chem* 2003; 278(36): 34141-9.
<http://dx.doi.org/10.1074/jbc.M303045200> PMID: 12773529
- [34] Pearlstein RA, Dickson CJ, Hornak V. Contributions of the membrane dipole potential to the function of voltage-gated cation channels and modulation by small molecule potentiators. *Biochim Biophys Acta Biomembr* 2017; 1859(2): 177-94.
<http://dx.doi.org/10.1016/j.bbmem.2016.11.005> PMID: 27836643
- [35] Fujiwara T, Oda K, Yokota S, Takatsuki A, Ikehara Y, Brefeldin A causes disassembly of the Golgi complex and accumulation of secretory proteins in the endoplasmic reticulum. *J Biol Chem* 1988; 263(34): 18545-52.
PMID: 3192548
- [36] Zou L-L, Ma J-L, Wang T, Yang T-B, Liu C-B. Cell-penetrating Peptide-mediated therapeutic molecule delivery into the central nervous system. *Curr Neuropharmacol* 2013; 11(2): 197-208.
<http://dx.doi.org/10.2174/1570159X11311020006> PMID: 23997754
- [37] Böttger R, Hoffmann R, Knappe D. Differential stability of therapeutic peptides with different proteolytic cleavage sites in blood, plasma and serum. *PLoS one* 2017; 12(6): e0178943.

- <http://dx.doi.org/10.1371/journal.pone.0178943>
- [38] Gorris HH, Bade S, Röckendorf N, *et al.* Rapid profiling of peptide stability in proteolytic environments. *Anal Chem* 2009; 81(4): 1580-6.
<http://dx.doi.org/10.1021/ac802324f> PMID: 19159331
- [39] Feng Z, Xu B. Inspiration from the mirror: D-amino acid containing peptides in biomedical approaches. *Biomol Concepts* 2016; 7(3): 179-87.
<http://dx.doi.org/10.1515/bmc-2015-0035> PMID: 27159920
- [40] Garton M, Nim S, Stone TA, Wang KE, Deber CM, Kim PM. Method to generate highly stable D-amino acid analogs of bioactive helical peptides using a mirror image of the entire PDB. *Proc Natl Acad Sci USA* 2018; 115(7): 1505-10.
<http://dx.doi.org/10.1073/pnas.1711837115> PMID: 29378946
- [41] Guo Z, Peng H, Kang J, Sun D. Cell-penetrating peptides: possible transduction mechanisms and therapeutic applications. *Biomed Rep* 2016; 4(5): 528-34.
<http://dx.doi.org/10.3892/br.2016.639> PMID: 27123243
- [42] Takeuchi T, Futaki S. Current understanding of direct translocation of arginine-rich cell-penetrating peptides and its internalization mechanisms. *Chem Pharm Bull* 2016; 64(10): 1431-7.
<http://dx.doi.org/10.1248/cpb.c16-00505> PMID: 27725497
- [43] Erickson SD, Simon JA, Still WC. Practical synthesis of a highly enantioselective receptor for peptides. *J Org Chem* 1993; 58(6): 1305-8.
<http://dx.doi.org/10.1021/jo00058a005>
- [44] Plazinska A, Plazinski W. Stereoselective binding of agonists to the β_2 -adrenergic receptor: insights into molecular details and thermodynamics from molecular dynamics simulations. *Mol Biosyst* 2017; 13(5): 910-20.
<http://dx.doi.org/10.1039/C6MB00814C> PMID: 28338133
- [45] Bechinger B, Seelig J. Interaction of electric dipoles with phospholipid head groups. A deuterium and phosphorus-31 NMR study of phloretin and phloretin analogs in phosphatidylcholine membranes. *Biochemistry* 1991; 30(16): 3923-9.
<http://dx.doi.org/10.1021/bi00230a017> PMID: 1850293
- [46] McLaurin J, Chakrabarty A. Characterization of the interactions of Alzheimer β -amyloid peptides with phospholipid membranes. *Eur J Biochem* 1997; 245(2): 355-63.
<http://dx.doi.org/10.1111/j.1432-1033.1997.t01-2-00355.x> PMID: 9151964
- [47] Peitzsch RM, Eisenberg M, Sharp KA, McLaughlin S. Calculations of the electrostatic potential adjacent to model phospholipid bilayers. *Biophys J* 1995; 68(3): 729-38.
[http://dx.doi.org/10.1016/S0006-3495\(95\)80253-5](http://dx.doi.org/10.1016/S0006-3495(95)80253-5) PMID: 7756540
- [48] Foroozandeh P, Aziz AA. Insight into cellular uptake and intracellular trafficking of nanoparticles. *Nanoscale Res Lett* 2018; 13(1): 339.
<http://dx.doi.org/10.1186/s11671-018-2728-6> PMID: 30361809
- [49] Salatin S, Yari Khosroushahi A. Overviews on the cellular uptake mechanism of polysaccharide colloidal nanoparticles. *J Cell Mol Med* 2017; 21(9): 1668-86.
<http://dx.doi.org/10.1111/jcmm.13110> PMID: 28244656
- [50] Jiao C-Y, Delaroche D, Burlina F, Alves ID, Chassaing G, Sagan S. Translocation and endocytosis for cell-penetrating peptide internalization. *J Biol Chem* 2009; 284(49): 33957-65.
<http://dx.doi.org/10.1074/jbc.M109.056309> PMID: 19833724
- [51] Madani F, Lindberg S, Langel U, Futaki S, Gräslund A. Mechanisms of cellular uptake of cell-penetrating peptides. *J Biophysics* 2011; 2011: 414729.
<http://dx.doi.org/10.1155/2011/414729>
- [52] Futaki S, Suzuki T, Ohashi W, *et al.* Arginine-rich peptides. An abundant source of membrane-permeable peptides having potential as carriers for intracellular protein delivery. *J Biol Chem* 2001; 276(8): 5836-40.
<http://dx.doi.org/10.1074/jbc.M007540200> PMID: 11084031
- [53] de Figueiredo IR, Freire JM, Flores L, Veiga AS, Castanho MARB. Cell-penetrating peptides: a tool for effective delivery in gene-targeted therapies. *IUBMB Life* 2014; 66(3): 182-94.
<http://dx.doi.org/10.1002/iub.1257> PMID: 24659560